Hindawi Publishing Corporation
EURASIP Journal on Wireless Communications and Networking
Volume 2007, Article ID 86031, 10 pages
doi:10.1155/2007/86031

Research Article

A Comprehensive Evaluation of Indoor Ranging Using Ultra-Wideband Technology

Camillo Gentile and Alfred Kik

Wireless Communication Technologies Group, National Institute of Standards and Technology, Gaithersburg, MD 20899-1070, USA

Received 1 May 2006; Revised 3 October 2006; Accepted 15 February 2007

Recommended by Arumugam Nallanathan

Ultra-wideband technology shows promise for precision ranging due to its fine time resolution to resolve multipath fading and the presence of lower frequencies in the baseband to penetrate walls. While a concerted effort has been conducted in the extensive modeling of the indoor UWB channel in recent years, to our knowledge only two papers have reported ranging performance, but for limited range and fixed bandwidth and center frequency. In principle, boosting power can guarantee connectivity between transmitter and receiver, but not precision due to the distorting effects of walls and other objects in the direct path. In order to gauge the limits of UWB ranging, we carry out 5000 measurements up to an unprecedented 45 m in non-line-of-sight conditions in four separate buildings with dominant wall material varying from sheet rock to steel. In addition, we report performance for varying bandwidth and center frequency of the system.

1. INTRODUCTION

Ultra-wideband (UWB) signals are characterized by a bandwidth greater than 500 MHz or one exceeding 20% of the center frequency of radiation [1, 2]. Such technology shows promise for indoor ranging due to its fine time resolution to resolve multipath fading and the presence of lower frequencies in the baseband to penetrate walls. The approval of the FCC unlicensed band from 3.1–10.6 GHz in 2002 has prompted a concerted effort in the extensive modeling of the indoor UWB channel in recent years. Irahhauten provides a comprehensive overview of indoor UWB measurements in the time and frequency domains [3]. Table 1 summarizes this overview, but augmented to include reported measurements to date. Most references in the table provide channel models characterized by path loss, small-scale fading, and delay spread. The most comprehensive of the models proposed by Molisch also includes frequency fading and clusters in the multipath profile. The latter gathers measurements conducted by separate parties with similar parameters to investigate not only three indoor environments, but also two outdoor environments and the body area network.

Emergency response systems in particular require that mobile rescue devices inside a building maintain connectivity to at least three base stations deployed outside to estimate their locations through triangulation of ranges [12]. In principle, boosting transmission power to levels above the FCC mask can ensure such connectivity for large buildings, however connectivity alone cannot guarantee precision due to the distorting effects of walls (and other objects) in the direct path. The number of wall interactions in general increases with range, leading to a degradation in performance due to the physical limits of the system. This evaluation quantifies the degradation up to an unprecedented 45 m due to the large dynamic range of our measurement system.

Similar to [8–11], we carry out 5000 measurements in the frequency domain from 2–8 GHz, however in a homogeneous fashion throughout four separate buildings. Rather than extract a channel model, we report the ranging performance based on time-of-flight estimation. To our knowledge, only Keignart and Scholtz have performed such a study [13–15], however to date no effort has been dedicated to the evaluation of this performance according to variation in system parameters. Specifically, the main contribution of this

Table 1: Overview of reported indoor UWB measurements.

	Prin. Investigator	f range	Environment	Range
Time	Yano [4]	1.25–2.75 GHz	office	17 m
	Cassioli et al. [2, 5, 6]	3.6–6 GHz	office	18 m
	Prettie et al. [7]	2–8 GHz	res.	20 m
Frequency	Kunisch and Pump [8]	1–11 GHz	office	10 m
	Keignart and Daniele [9]	2–6 GHz	office/res.	20 m
	Ghassemzadeh et al. [10]	2–8 GHz	res./commercial	15 m
	Molisch et al. [11]	3–10 GHz	res./	28 m
			industrial/office	20 m

paper is a study of the relationship between range error and the following.

(i) *Bandwidth*: precision increases with bandwidth, but carries diminishing returns with the additional expense.

(ii) *Center frequency*: lower frequencies penetrate materials better.[1]

(iii) *Construction material*: compare performance with typical building construction materials varying as sheet rock (easy), plaster, cinder block, to steel (most difficult) to gauge lower and upper bounds on the technology, rather than with building layout (i.e., office, residential typically have the same wall materials).

(iv) *Long range*: the high dynamic range of our system allows us to span 45 m and examine the limits in the technology inherent to the interaction with up to 12 walls.

We also compute the path loss for all the experiments to render the results independent of our particular transmitter power and receiver sensitivity.

The paper reads as follows: Section 2 describes the technique for channel measurement in the frequency domain used to estimate range, and Section 3 provides the details of our equipment setup. Section 4 outlines our suite of measurements and presents the results both through statistical measures and in graphical format, followed by conclusions in the last section.

2. PRELIMINARIES

2.1. The indoor propagation channel

The conventional model for the indoor propagation channel consists of an impulse train representing K multipath arrivals indexed through k [17]

$$h(t) = \sum_{k=0}^{K-1} \alpha_k \delta(t - \tau_k), \tag{1}$$

where τ_k denotes the delay of the arrival in propagating between the transmitter and the receiver, and α_k denotes the complex-valued amplitude which accounts for both attenuation and phase change due to reflection, diffraction, and other specular effects introduced by walls (and other objects) on its path.

Figure 1(a) displays a typical impulse response for *line-of-sight* (LOS) conditions between the transmitter and the receiver. Ranging systems based on *time-of-flight* estimate the delay τ_f associated with the arrival of the first impulse in the response, or *leading edge*. Since the signal propagates at the speed of light c in free space, the estimated range between the radios is $c \cdot \tau_f$. Indoor propagation delivers many and closely-packed arrivals to the receiver inherent to the smaller dimensions of objects compared to outdoors. Ultra-wideband transmitters send pulses sufficiently narrow in time to allow for path resolution at the receiver, avoiding overlap of the pulses which may otherwise combine in a destructive manner and render poor results. Even though UWB can successfully isolate multipath arrivals, the interaction of the signals with the walls distorts the signal. In *non-line-of-sight* (NLOS) conditions such as in Figure 1(b), the leading-edge path propagating through walls may appear attenuated with respect to another reflected path, or even buried below the noise floor of the channel. Even if detectable, the leading edge propagates through walls slower than the speed of light, adding an irrecoverable delay with each in the estimation of τ_f since the number of walls and construction material are unknown a priori: sheet rock (cinder block) introduces an additional delay of 1.8 ns/m wall (3.4 ns/m wall) for a total range error of 54 cm (102 cm) through 10 walls typically 10 cm thick [18]. This phenomenon places a physical limit on the performance of the system.

The impulse response of the channel in (1) has a frequency response

$$H(f) = \sum_{k=0}^{K-1} \alpha_k e^{-j2\pi f \tau_k} \tag{2}$$

suggesting that the channel can be characterized through frequency measurements. We compute the frequency response $H(f) = Y(f)/X(f)$ by transmitting tones $X(f)$ across the channel at discrete values of f and then measuring $Y(f)$ at the receiver. Characterizing the channel in the frequency domain offers an important advantage over transmitting a fixed

[1] Cassioli et al. [16] performed a similar study of the relationship between path loss and center frequency.

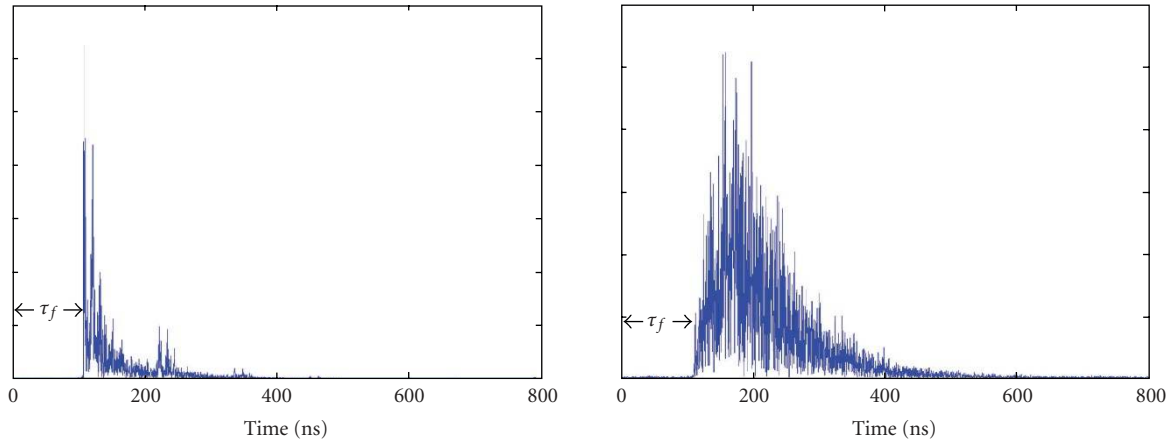

(a) Line-of-sight conditions

(b) Non-line-of-sight conditions

Figure 1: The impulse response of the channel.

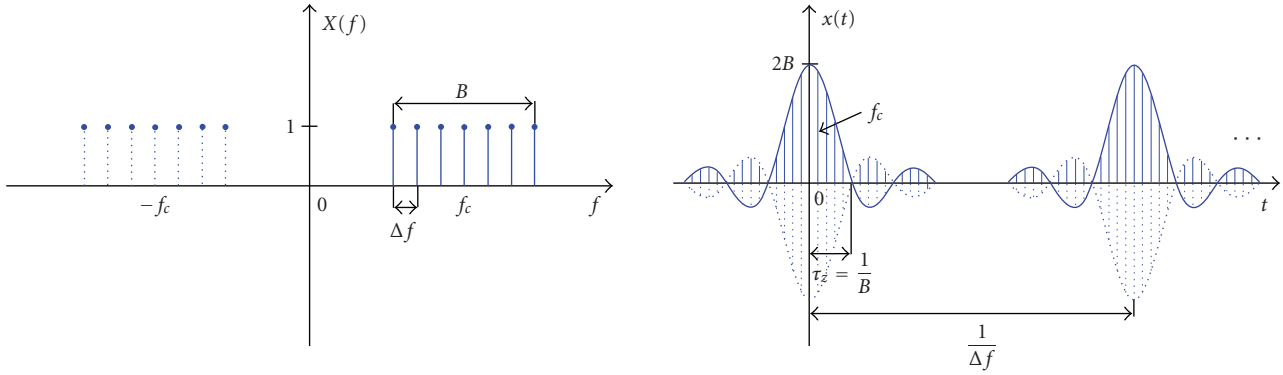

(a) Frequency domain

(b) Time domain

Figure 2: The signal emitted at the transmitter.

pulse in the time domain and recording the impulse response directly: once we sweep the 2–8 GHz band of interest, a subband with bandwidth B and the center frequency f_c can be selected a posteriori in varying the parameters of the system. The discrete frequency spectrum $X(f)$ in Figure 2(a) translates to the time domain as the periodic sinc pulse $x(t)$ in Figure 2(b) with revolution $1/\Delta f$ modulated at f_c [19]. The bandwidth controls the width of the pulse defined through the first zero-crossing $\tau_z = 1/B$, and in turn controls the multipath resolution of the system. Choosing $\Delta f = 1.25$ MHz allows for a maximum multipath spread of 800 nanoseconds, which proves sufficient throughout all four buildings for the arrivals to subside within one period and avoid time aliasing. The corresponding impulse response can be recovered through the inverse discrete fourier transform (IDFT) [20]

$$h(t) = \frac{1}{2} \sum_{l=0}^{B/\Delta f} H(f) e^{j2\pi f t} + H^*(f) e^{-j2\pi f t}, \tag{3}$$

where $f = f_c - (B/2) + l \cdot \Delta f$. The average path loss of the channel is expressed as [10]

$$\mathrm{PL} = \frac{1}{1 + (B/\Delta f)} \sum_{l=0}^{B/\Delta f} |H(f)|^2. \tag{4}$$

2.2. Time-of-flight estimation

In order to estimate τ_f, we first apply a Kaiser filter to the subband; this reduce the sidelobes of the sinc pulse after taking the IDFT. While super-resolution techniques [19, 21] in generating the impulse response show a significant improvement over conventional techniques such as the IDFT for smaller bandwidths, as us, the same authors witnessed no such improvement for bandwidths in excess of 0.2 GHz, those considered in this study.

The *kurtosis* has been used in the literature for signal-to-noise estimation in digital communication systems [22]. The key strength of this measure lies in its channel invariance, enabling application of the system with no prior knowledge of the environment. In theory, it indicates the Gaussian

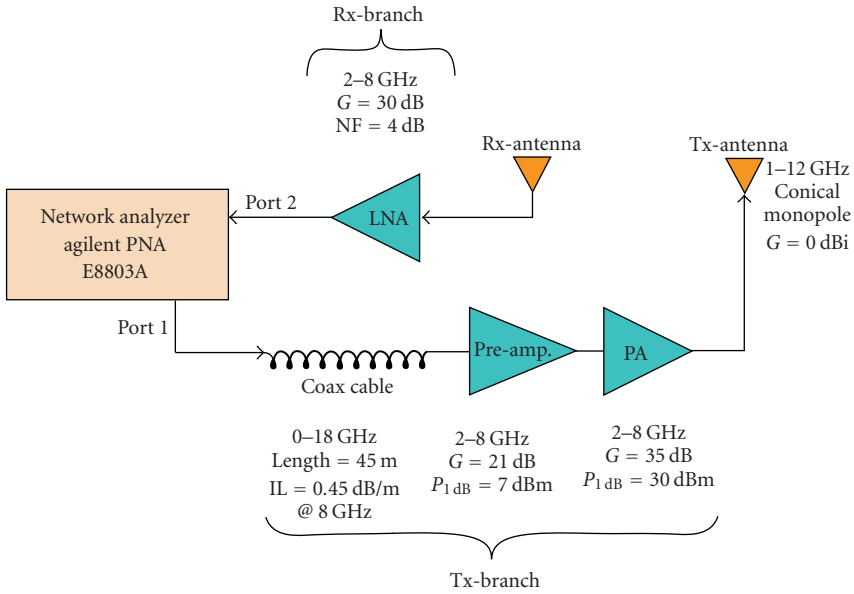

(a) Block diagram

(b) Photograph

Figure 3: The measurement system using the vector network analyzer.

unlikeness of a window $w[t]$ centered at t when its value defined as

$$\kappa(w[t]) = \frac{E(w^4[t])}{E^2(w^2[t])} \tag{5}$$

exceeds 3. Under the fair assumption of Gaussian noise in the channel [23], an effective thresholding technique recently published [24] detects the presence of a signal by computing the kurtosis of a fixed-length sliding window originating at the beginning of the impulse response. It selects the leading edge as the first time sample $t = \tau_f$ in the profile when $\kappa(w[t])$ exceeds a threshold. We performed a two-dimensional search in function of the window size (5–30) and the threshold (2–7) to find the optimal parameters of 8 and 4.4, respectively, which minimized the cumulative range error over all the measurements recorded. Other papers in literature propose alternative thresholding techniques for estimating τ_f in UWB ranging tailored to their specific measurement systems [15, 25, 26].

3. MEASUREMENT SYSTEM

Figure 3 displays the block diagram and photograph of our measurement system. The vector network analyzer (VNA) emits a series of tones with frequency f at Port 1 and measures the relative amplitude and phase $S_{21}(f)$ at Port 2, providing automatic phase synchronization between the two ports. The synchronization translates to a common time reference for the transmitted and received signals. The long cable enables variable positioning of the conical monopole antennas from each other throughout the test area. The preamplifier and power amplifier on the transmit branch boost the signal such that it radiates at approximately 30 dBm from the antenna. After it passes through the channel, the low-noise amplifier (LNA) on the receiver branch boosts the signal above the noise floor of Port 2 before feeding it back.

The $S_{21}(f)$-parameter of the network in Figure 3 can be expressed as a product of the Tx-branch, the Tx-antenna, the propagation channel, the Rx-antenna, and the Rx-branch

$$\begin{aligned} S_{21}(f) &= H_{\text{Tx}}^{\text{bra}}(f) \cdot H_{\text{Tx}}^{\text{ant}}(f) \cdot H(f) \cdot H_{\text{Rx}}^{\text{ant}}(f) \cdot H_{\text{Rx}}^{\text{bra}}(f) \\ &= H_{\text{Tx}}^{\text{bra}}(f) \cdot \underbrace{H_{\text{Tx}}^{\text{ant}}(f) \cdot H_{\text{Rx}}^{\text{ant}}(f)}_{H^{\text{ant}}(f)} \cdot H(f) \cdot H_{\text{Rx}}^{\text{bra}}(f). \end{aligned} \tag{6}$$

The frequency response of the channel H is extracted by individually measuring the transmission responses $H_{\text{Tx}}^{\text{bra}}$, $H_{\text{Rx}}^{\text{bra}}$, and H^{ant} in advance and de-embedding them from (6). Measuring the characteristics of the antennas on a flat open field with dimensions exceeding 100 m × 100 m reduced ambient multipath to a single ground bounce which we removed by placing electromagnetic absorbers on the ground between the antennas. We separated the antennas by a distance of 1.5 m to avoid the near-field effects and spatially averaging them through rotation with respect to each other every ten degrees [27]. Their height was set to 1.7 m (average human height).

Note in particular the following implementation considerations.

(i) To account for the frequency-dependent loss in the long cable when operating across such a large bandwidth, we ramped up the emitted power at Port 1 with increasing frequency to radiate from the antenna at approximately 30 dBm across the whole band.

(ii) We removed the LNA from the network in experiments with range below 10 m to protect it from overload and also avert its operation in the nonlinear region.

Table 2: Experiments conducted in measurement campaign.

Building	Wall material	LOS range (10)	NLOS range (40)
NIST North	Sheet rock/ aluminum studs	1.2–24.3 m	1.7–40.7 m max wall no.: 12
Child Care	Plaster/ wooden studs	2.0–15.7 m	4.7–33.0 m max wall no.: 7
Sound	Cinder block	3.4–45.0 m	5.9–40.8 m max wall no.: 9
Plant	Steel	2.9–43.7 m	4.9–44.0 m max wall no.: 8

(iii) To extend the dynamic range of our system, we exploited the configurable test set option of the VNA to reverse the signal path in the coupler of Port 2 and bypass the 12 dB loss associated with the coupler arm. The dynamic range of the propagation channel corresponds to 144 dB as computed through [9] for an IF bandwidth of 1 kHz and a SNR of 10 dB at the receiver.

(iv) To account for the small-scale effects in the measurements, for each experiment we centered a 5×5 grid constructed from a wooden plank on the floor about the nominal location of the receiver antenna. The distance between the grid points was 15 cm, corresponding to a full wavelength at 2 GHz, ensuring spatial independence between the measured points for a total of 25 subexperiments.

4. EXPERIMENTAL SETUP AND RESULTS

4.1. Experimental setup

The measurement campaign was conducted in four separate buildings on the NIST campus in Gaitherburg, Maryland each constructed from a dominant wall material varying from sheet rock (easy) to steel (most difficult). This variation allows gauging lower and upper bounds on the performance of indoor ranging using UWB technology. Table 2 summarizes the 50 experiments in each building (10 LOS and 40 NLOS), including the maximum number of walls separating the transmitter and receiver.

As an example, consider the plan of *NIST North* in Figure 4, the experiments were drawn from the two sets of 31 transmitter locations and 5 receiver locations, indicated by the solid and empty circles, respectively, to the end of achieving a uniform distribution in range in both LOS and NLOS conditions. The solid line identifies the experiment with the longest range traversing 12 walls between the transmitter and receiver. For the most part, the measurements were taken after working hours to minimize any disturbance due to the movement of personnel throughout the buildings.

4.2. Results

The range error of a subexperiment, defined as the absolute difference between the estimated range and the ground-truth range at the corresponding point on the grid, serves as a performance measure of the system. The ground-truth ranges were computed by pinpointing the nominal locations of the transmitter and receiver with a laser tape for each experiment in the campaign, and automatically extrapolating the 25 locations on the grid using a computer-aided design (CAD) model of each building layout, for a total of 5000 measurements (50 experiments $\times$25 subexperiments $\times$4 buildings).

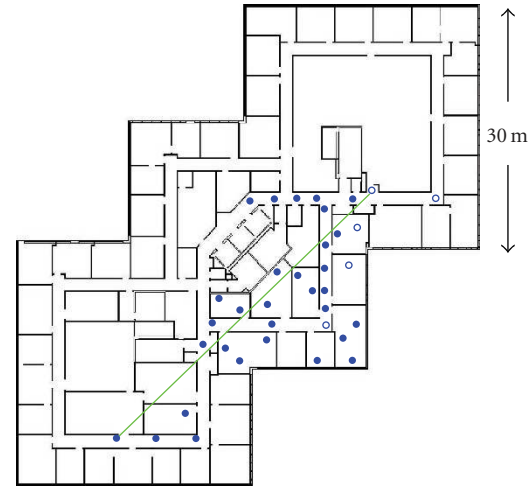

Figure 4: The plan of the *NIST North* building.

We reduce the 25 range errors on the grid to an average range error for each experiment. Table 3 reports the statistics of the average range errors for the experiments associated with each cross-labeled scenario in the following format:

$$\boxed{\begin{array}{c}\mu_e(cm),\ \sigma_e(cm)\\ \min_e(cm),\ \max_e(cm)\\ \mathrm{PL}_0,\ \gamma\end{array}} \qquad (*)$$

where μ_e, σ_e, $\min_e$ and $\max_e$ denote the mean, standard deviation, minimum, and maximum values of the average range errors; PL_0 and γ, respectively, characterize the reference loss at $r_0 = 1$ m and the exponent of the single-slope path loss model [10]

$$\mathrm{PL}(r)(dB) = \mathrm{PL}_0 + 10\gamma \log_{10}\left(\frac{r}{r_0}\right) \qquad (7)$$

fit to the data points generated from (4) in function of the ground-truth range r. Reporting the path loss for each scenario disassociates the results from our particular transmitter power and receiver sensitivity, barring interference.

Figure 5(a) illustrates the average range error (cm) versus the nominal ground-truth range (m) for the LOS experiments in *NIST North* at $f_c = 5$ GHz while varying $B = \{0.5, 1, 2, 4, 6\}$ GHz, the latter multiplexed on the abscissa. The color of the point represents the path loss (dB) in reference to the legend: the strength of the first arrival decreases with range, but so long as it remains above the receiver sensitivity, no matter how much, it can be detected without degrading the system performance. It follows that no obvious

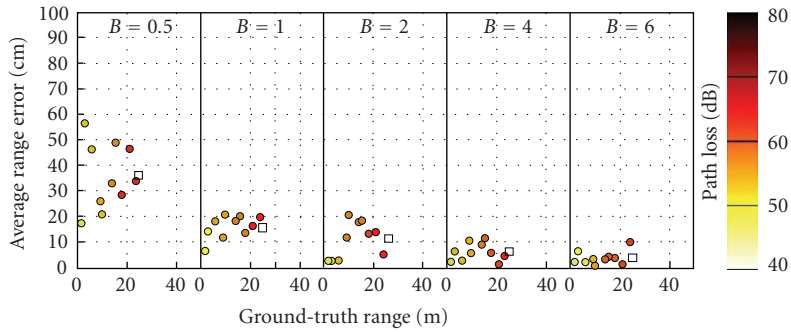

(a) *NIST North*, LOS, $f_c = 5$ GHz

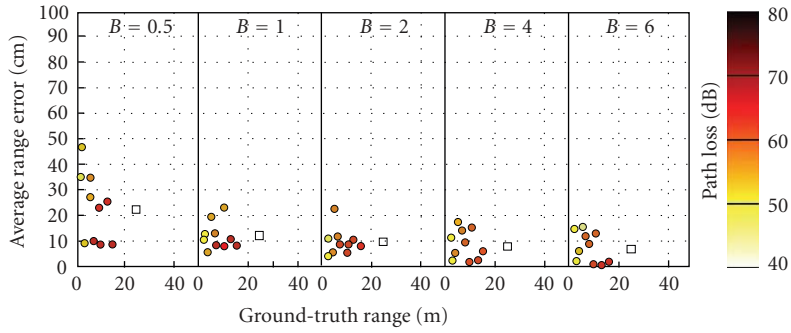

(b) *Child Care*, LOS, $f_c = 5$ GHz

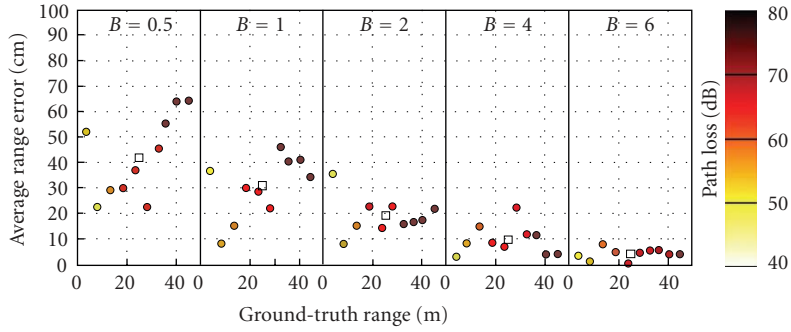

(c) *Sound*, LOS, $f_c = 5$ GHz

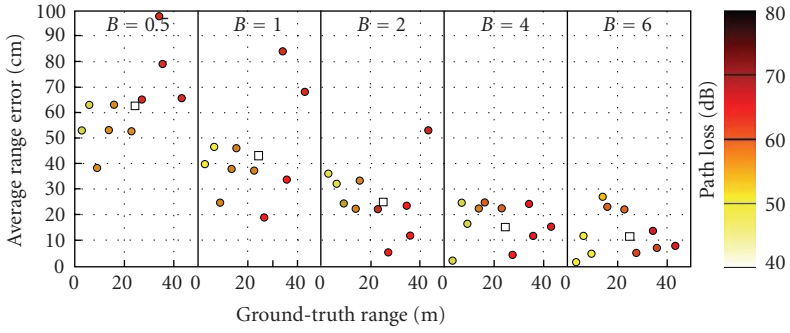

(d) *Plant*, LOS, $f_c = 5$ GHz

FIGURE 5: Range error (cm) versus ground-truth range (m) while varying bandwidth B (GHz) in line-of-sight conditions.

Table 3: Statistical results for experiments.

	Building	$B = 0.5$	$B = 1$			$B = 2$			$B = 4$			$B = 6$
		$f_c = 5$	$f_c = 3$	$f_c = 5$	$f_c = 7$	$f_c = 3$	$f_c = 5$	$f_c = 7$	$f_c = 4$	$f_c = 5$	$f_c = 6$	$f_c = 5$
LOS	*NIST North*	36, 13	15, 5	15, 5	25, 13	6, 6	11, 7	14, 9	6, 4	6, 3	6, 3	4, 3
		17, 56	6, 25	6, 21	8, 47	1, 20	2, 21	1, 27	1, 12	1, 11	2, 12	1, 10
		42, 1.6	42, 1.3	42, 1.5	42, 1.6	40, 1.4	43, 1.5	43, 1.6	41, 1.4	44, 1.3	43, 1.5	42, 1.4
	Child Care	23, 14	14, 8	12, 6	15, 10	10, 5	10, 5	11, 7	8, 6	8, 6	9, 7	7, 6
		9, 47	6, 24	6, 23	6, 35	5, 20	4, 23	5, 25	2, 18	2, 18	1, 18	0, 16
		43, 2.2	40, 2.2	44, 2.1	44, 2.1	38, 2.3	45, 1.8	46, 2.0	41, 2.1	45, 1.8	45, 1.9	42, 2.1
	Sound	43, 16	23, 10	31, 12	34, 12	12, 7	19, 9	22, 11	7, 5	10,6	7, 4	4, 2
		23, 64	9, 38	9, 46	22, 57	0, 23	8, 36	8, 44	1, 14	4, 22	1, 15	0, 8
		34, 2.4	37, 1.8	33, 2.5	28, 2.8	34, 2.0	34, 2.4	29, 2.7	34, 2.1	35, 2.2	31, 2.6	32, 2.3
	Plant	62, 20	35, 11	43, 22	40, 15	17, 8	25, 15	22, 12	15, 11	15, 8	12, 8	9, 9
		38, 98	21, 52	19, 83	11, 53	4, 24	5, 53	4, 38	2, 30	2, 24	2, 22	1, 27
		35, 2.0	36, 1.7	36, 2.0	34, 2.2	34, 1.7	37, 1.9	34, 2.1	35, 1.8	37, 1.8	35, 2.0	35, 1.9
NLOS	*NIST North*	103, 67	59, 29	58, 28	60, 26	38, 21	39, 17	45, 21	27, 11	28, 10	27, 10	24, 9
		16, 355	10, 145	18, 150	17, 160	5, 85	7, 85	11, 130	4, 51	4, 52	4, 50	1, 41
		27, 4.6	25, 4.5	27, 4.6	23, 4.9	21, 4.7	27, 4.6	25, 4.8	24, 4.6	27, 4.5	26, 4.7	24, 4.6
	Child Care	111, 58	65, 46	71, 39	79, 39	46, 39	52, 34	59, 39	44, 32	39, 31	47, 40	38, 33
		23, 259	10, 173	10, 167	11, 157	4, 157	5, 130	4, 150	3, 132	4, 119	3, 158	2, 133
		17, 6.4	18, 5.8	17, 6.4	13, 6.9	18, 5.6	17, 6.4	14, 7.0	19, 5.7	18, 6.3	16, 6.6	19, 5.8
	Sound	171, 88	116, 62	127, 70	147, 97	89, 59	94, 70	117,78	78, 65	86, 84	103, 68	84, 82
		34, 363	21, 292	32, 295	32, 398	17, 306	20, 325	19, 427	7, 309	8, 244	7, 236	6, 157
		29, 5.2	28, 4.8	30, 5.1	30, 5.3	26, 4.8	30, 5.1	33, 5.2	28, 4.9	31, 5.0	31, 5.1	29, 4.9
	Plant	537, 331	490, 350	483, 345	522, 347	444, 326	466, 342	531, 371	432, 359	408, 330	450, 378	350, 260
		28, 1170	32, 1149	23, 1110	24, 1161	39, 1096	37, 1125	38, 1187	43, 1160	41, 1199	43, 1184	44, 948
		38, 3.2	39, 2.8	38, 3.2	38, 3.3	37, 2.8	39, 3.2	39, 3.3	38, 2.9	40, 3.0	39, 3.2	39, 2.9

correlation exists between error and range in line-of-sight conditions. The error lies within 10 cm at $B = 6$ GHz up to a range of 45 m. The mean μ_e of each scenario from Table 3 also appears on the plot as a hollow square to highlight the trend in parameter variation: performance improves significantly with increasing bandwidth, but at diminishing returns: μ_e drops from 36 to 15 cm from $B = 0.5$ to 1 GHz, but only from 6 to 4 cm from $B = 4$ to 6 GHz. This phenomenon holds true throughout all LOS and NLOS scenarios in all buildings as a consequence of the relationship $\tau_z = 1/B$ since $d\tau_z/dB = -1/B^2$, the same increment in bandwidth dB at a higher operating bandwidth B results in a smaller decrement in the pulse width $d\tau_z$ which controls the resolution performance of the system. The LOS experiments in Figures 5(b)–5(d) in the other three buildings exhibit similar behavior as in *NIST North*. Overall the system delivers $\mu_e = 6$ cm at $B = 6$ GHz throughout all four buildings tested.

The plots in Figure 6 display the NLOS scenarios in *NIST North*, *Child Care*, and *Sound* at $f_c = 5$ GHz while varying $B = \{0.5, 1, 2, 4, 6\}$ GHz. While notably worse than the LOS experiments, the error still lies within 41 cm (1% error as a percentage of the ground-truth range) in *NIST North* and yields $\mu_e = 24$ cm at 6 GHz. The mean μ_e increases to 38 and 84 cm in *Child Care* and *Sound*, respectively, with most of the errors below 100 cm (3%) and 150 cm (4%); considering that the signal traverses up to 40 m and 9 walls in these two buildings, the results fare quite well, especially since computing location by triangulating three or more ranges can reduce the location error by an order of magnitude with respect to the range error [12]. Despite the small path loss in *Plant* (not shown) due to the favorable properties of the walls which behave as waveguides, the system provides $\mu_e = 350$ cm and an error less than 390 cm only up to 15 m at $B = 6$ GHz, clearly manifesting the impenetrable properties of metal by the direct path.

In most scenarios across the four buildings, the error increases substantially at higher center frequencies due to larger associated path losses as quantified in Table 3; this phenomenon surfaces more in *Sound* due to thicker walls than in *NIST North* and *Child Care*. The plots in Figure 7 display the NLOS scenarios in the *Sound* building for $B = \{1, 2, 4\}$ GHz while varying f_c, the latter multiplexed on the abscissa. For all three bandwidths, μ_e increases about 30 cm from the lowest to the highest center frequency. On the contrary, μ_e remains relatively constant while varying f_c with an unobstructed direct path in the LOS scenarios.

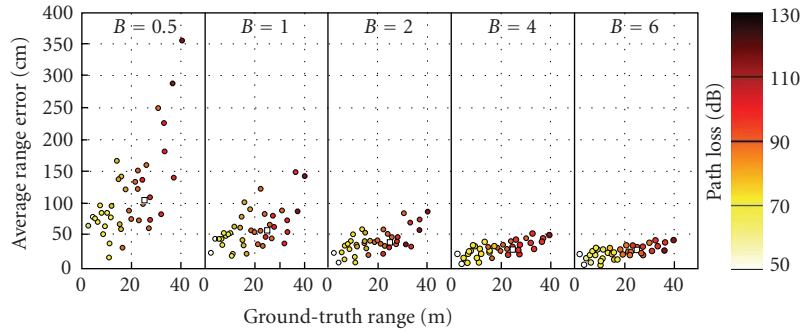

(a) *NIST North*, NLOS, $f_c = 5$ GHz

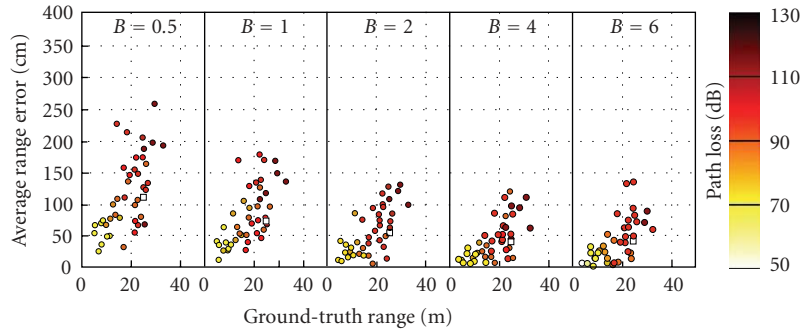

(b) *Child Care*, NLOS, $f_c = 5$ GHz

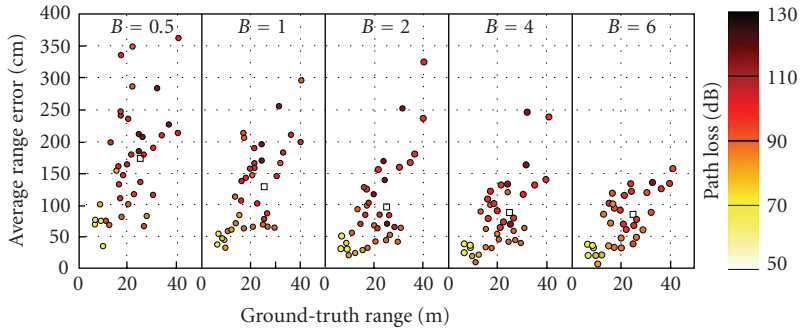

(c) *Sound*, NLOS, $f_c = 5$ GHz

Figure 6: Range error (cm) versus ground-truth range (m) while varying bandwidth B (GHz) in nonline-of-sight conditions.

In order to quantify the small-scale effects in the measurements, we also compute the standard deviation of the 25 range errors on the grid for each experiment. The standard deviation varied between 0.5 to 1 cm in LOS conditions for all four buildings. The mean of the standard deviation over the ensemble of experiments in NLOS conditions rose to 3, 5, 11, and 70 cm for *NIST North*, *Child Care*, *Sound*, and *Plant*, respectively. No apparent trend existed in the standard deviation as a function of range as opposed to the increasing average range error observed in the figures as a function of range.

5. CONCLUSIONS

Our nominal ranging system at 6 GHz bandwidth and 5 GHz center frequency delivers a mean range error of 6 cm in line-of-sight conditions up to a range of 45 m throughout all four buildings tested. This error increases to 24, 38, and 84 cm for sheet rock, plaster, and cinder block wall materials, respectively, in non-line-of-sight conditions; the system ranges within 390 cm up to 15 m in the steel building, but the performance degrades rapidly thereafter. The ranging precision improves significantly when raising the bandwidth from

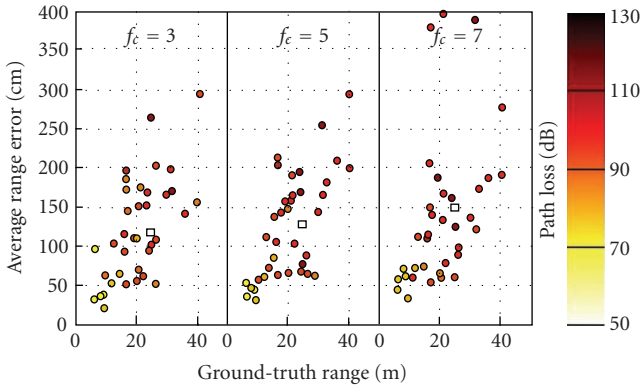

(a) *Sound*, NLOS, $B = 1$ GHz

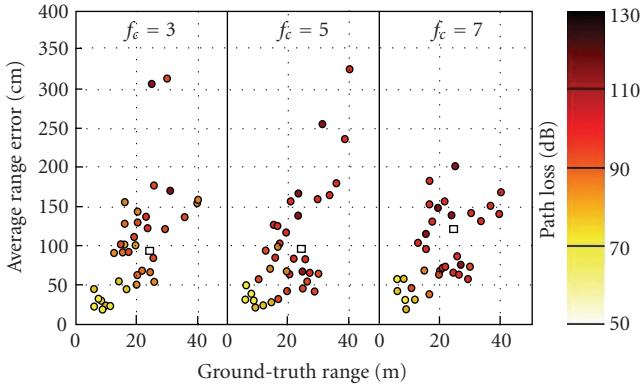

(b) *Sound*, NLOS, $B = 2$ GHz

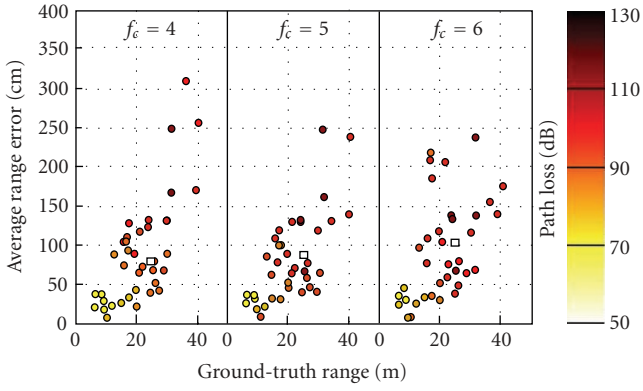

(c) *Sound*, NLOS, $B = 4$ GHz

Figure 7: Range error (cm) versus ground-truth range (m) while varying center frequency f_c (GHz) in non-line-of-sight conditions.

0.5 GHz to 4 GHz, but at a diminishing rate, and shows virtually no further improvement at 6 GHz. The error increases up to 31 cm from a center frequency of 3 to 7 GHz due to larger path loss of the latter with an obstructed direct path, but remains fairly constant in line-of-sight conditions.

REFERENCES

[1] A. F. Molisch, "Ultrawideband propagation channels-theory, measurement, and modeling," *IEEE Transactions on Vehicular Technology*, vol. 54, no. 5, pp. 1528–1545, 2005.

[2] D. Cassioli, M. Z. Win, and A. F. Molisch, "The ultra-wide bandwidth indoor channel: from statistical model to simulations," *IEEE Journal on Selected Areas in Communications*, vol. 20, no. 6, pp. 1247–1257, 2002.

[3] Z. Irahhauten, H. Nikookar, and G. J. M. Janssen, "An overview of ultra wide band indoor channel measurements and modeling," *IEEE Microwave and Wireless Components Letters*, vol. 14, no. 8, pp. 386–388, 2004.

[4] S. M. Yano, "Investigating the ultra-wideband indoor wireless channel," in *The 55th of IEEE Vehicular Technology Conference (VTC '02)*, vol. 3, pp. 1200–1204, Birmingham, Ala, USA, May 2002.

[5] A. Durantini, W. Ciccognani, and D. Cassioli, "UWB propagation measurements by PN-sequence channel sounding," in *IEEE International Conference on Communications (ICC '04)*, vol. 6, pp. 3414–3418, Paris, France, June 2004.

[6] A. Durantini and D. Cassioli, "A multi-wall path loss model for indoor UWB propagation," in *The 61st of IEEE Vehicular Technology Conference (VTC '05)*, vol. 1, pp. 30–34, Stockholm, Sweden, May-June 2005.

[7] C. Prettie, D. Cheung, L. Rusch, and M. Ho, "Spatial correlation of UWB signals in a home environment," in *IEEE Conference on Ultra Wideband Systems and Technologies (UWBST '02)*, pp. 65–69, Baltimore, Md, USA, May 2002.

[8] J. Kunisch and J. Pump, "Measurement results and modeling aspects for the UWB radio channel," in *IEEE Conference on Ultra Wideband Systems and Technologies (UWBST '02)*, pp. 19–24, Baltimore, Md, USA, May 2002.

[9] J. Keignart and N. Daniele, "Subnanosecond UWB channel sounding in frequency and temporal domain," in *IEEE Conference on Ultra Wideband Systems and Technologies (UWBST '02)*, pp. 25–30, Baltimore, Md, USA, May 2002.

[10] S. S. Ghassemzadeh, L. J. Greenstein, T. Sveinsson, A. Kavčić, and V. Tarokh, "UWB delay profile models for residential and commercial indoor environments," *IEEE Transactions on Vehicular Technology*, vol. 54, no. 4, pp. 1235–1244, 2005.

[11] A. F. Molisch, K. Balakrishnan, D. Cassioli, et al., "A comprehensive model for ultrawideband propagation channels," in *IEEE Global Telecommunications Conference (GLOBECOM '05)*, vol. 6, pp. 3648–3653, St. Louis, Mo, USA, November-December 2005.

[12] C. Gentile, "Sensor location through linear programming with triangle inequality constraints," in *IEEE International Conference on Communications (ICC '05)*, vol. 5, pp. 3192–3196, Seoul, Korea, May 2005.

[13] B. Denis, J. Keignart, and N. Daniele, "Impact of NLOS propagation upon ranging precision in UWB systems," in *IEEE Conference on Ultra Wideband Systems and Technologies (UWBST '03)*, pp. 379–383, Reston, Va, USA, November 2003.

[14] B. Denis and N. Daniele, "NLOS ranging error mitigation in a distributed positioning algorithm for indoor UWB ad-hoc networks," in *International Workshop on Wireless Ad-Hoc Networks (IWWAN '04)*, pp. 356–360, Oulu, Finland, May-June 2004.

[15] J.-Y. Lee and R. A. Scholtz, "Ranging in a dense multipath environment using an UWB radio link," *IEEE Journal on Selected Areas in Communications*, vol. 20, no. 9, pp. 1677–1683, 2002.

[16] D. Cassioli, A. Durantini, and W. Ciccognani, "The role of path loss on the selection of the operating bands of UWB systems," in *The 15th of IEEE International Symposium on Personal, Indoor and Mobile Radio Communications (PIMRC '04)*, vol. 4, pp. 2787–2791, Barcelona, Spain, September 2004.

[17] H. Hashemi, "Indoor radio propagation channel," *Proceedings of the IEEE*, vol. 81, no. 7, pp. 943–968, 1993.

[18] A. Muqaibel, A. Safaai-Jazi, A. Bayram, A. M. Attiya, and S. M. Riad, "Ultrawideband through-the-wall propagation," *IEE Proceedings: Microwaves, Antennas & Propagation*, vol. 152, no. 6, pp. 581–588, 2005.

[19] X. Li and K. Pahlavan, "Super-resolution TOA estimation with diversity for indoor geolocation," *IEEE Transactions on Wireless Communications*, vol. 3, no. 1, pp. 224–234, 2004.

[20] L. Hentilä, V. Hovinen, and M. Hämäläinen, "Sub-band analysis in UWB radio channel modeling," in *Proceedings of Nordic Radio Symposium/Finnish Wireless Communications Workshop (NRS/FWCW '04)*, pp. 1–5, Oulu, Finland, August 2004.

[21] G. Morrison and M. Fattouche, "Super-resolution modeling of the indoor radio propagation channel," *IEEE Transactions on Vehicular Technology*, vol. 47, no. 2, pp. 649–657, 1998.

[22] R. Matzner and K. Letsch, "SNR estimation and blind equalization (deconvolution) using the kurtosis," in *Proceedings of IEEE-IMS Workshop on Information Theory and Statistics (WITS '94)*, p. 68, Alexandria, Va, USA, October 1994.

[23] I. Guvenc and Z. Sahinoglu, "Threshold-based TOA estimation for impulse radio UWB systems," in *Proceedings of IEEE International Conference on Ultra-Wideband, Conference (ICU '05)*, pp. 420–425, Zurich, Switzerland, September 2005.

[24] I. Guvenc and Z. Sahinoglu, "Threshold selection for UWB TOA estimation based on kurtosis analysis," *IEEE Communications Letters*, vol. 9, no. 12, pp. 1025–1027, 2005.

[25] C. Falsi, D. Dardari, L. Mucchi, and M. Z. Win, "Time of arrival estimation for UWB localizers in realistic environments," *EURASIP Journal on Applied Signal Processing*, vol. 2006, Article ID 32082, 13 pages, 2006.

[26] Z. N. Low, J. H. Cheong, C. L. Law, W. T. Ng, and Y. J. Lee, "Pulse detection algorithm for line-of-sight (LOS) UWB ranging applications," *IEEE Antennas and Wireless Propagation Letters*, vol. 4, no. 1, pp. 63–67, 2005.

[27] S. Zwierzchowski and P. Jazayeri, "A systems and network analysis approach to antenna design for UWB communications," in *Proceedings of IEEE International Symposium on Antennas and Propagation Society (APS '03)*, vol. 1, pp. 826–829, Columbus, Ohio, USA, June 2003.